LA-UR-83-98

Los Alamos National Laboratory is operated by the University of California for the United States Department of Energy under contract W-7405-ENG-36.

TITLE: EMPIRICAL CHARACTERIZATION OF OIL SHALE CRATERING EXPERIMENTS

AUTHOR(S): C. L. Edwards, J. L. Craig, and K. Lombardo

SUBMITTED TO: Society of Explosives Engineers
9th Annual Conference on Explosives and Blasting Techniques



Los Alamos Los Alamos National Laboratory
Los Alamos, New Mexico 87545

FORM NO. 836 R4
ST. NO. 2629 5/81

# EMPIRICAL CHARACTERIZATION OF OIL SHALE CRATERING EXPERIMENTS

by

C. L. Edwards, J. L. Craig, and K. Lombardo
Geophysics Group
Los Alamos National Laboratory
Los Alamos, New Mexico 87545

ABSTRACT

Numerous small- and intermediate-size cratering experiments have been conducted in Piceance Creek Basin oil shale at the Colony and Anvil Points oil shale mines near Rifle, Colorado. The purpose of these experiments was to evaluate scaling as a tool to infer the behavior of large-scale tests from small-scale experiments, to calibrate the hydrodynamic computer codes used to model explosive fragmentation of oil shale, and to investigate the influence of bedding plane orientation, natural joints, fractures, and the grade of oil shale on rock fragmentation.

The small tests were made using PETN and RDX explosive with charge sizes of a few grams. The intermediate-sized tests used ANFO or TNT explosives with charge sizes of 5 to 100 kg. Crater dimensions were measured on all experiments. Crater volumes were calculated from screened rubble volumes on the intermediate-scale experiments and measured directly on the small-scale experiments. Fragment size distributions were measured on most of the intermediate-sized tests and on several of the small-scale experiments.

The analyses of these cratering data show: (1) small-scale cratering tests can be used to qualitatively predict the kinds of geologic interactions that will influence a larger-scale experiment; (2) the site specific geology plays a dominant role in the formation of the crater; (3) small flaws and fractures influence crater development and particle size distributions in small-scale craters in the same manner that joint and fracture systems

References and illustrations following text.

influence intermediate-scale experiments; (4) complex site geology causes increases in the critical and optimum depths of burial and changes the symmetry of the crater; and (5) small- and intermediate-scale cratering experiments can be used to calibrate hydrodynamic computer codes if great care is used to identify the effect of site specific geology.

## INTRODUCTION

As part of the Department of Energy (DOE) Oil Shale Fragmentation Program, during the period 1978 through 1980, the Los Alamos National Laboratory conducted 19 single and multiple borehole cratering experiments at the Colony Oil Shale Mine near Parachute, Colorado. Subsequently, Los Alamos, in conjunction with Science Applications Inc. (SAI), participated in an extensive program of explosive rubbling experiments at the DOE oil shale mine at Anvil Points, Colorado. An additional 275 small-scale experiments (less than 10 g of explosive) were performed in the laboratory and in the Colony and Anvil Points mines.

The purpose of these experiments was to: (1) determine if small-scale tests could qualitatively predict the kinds of geologic interactions that influence larger-scale experiments; (2) evaluate how and to what extent site geology affected the rock fragmentation and crater formation; (3) determine what scaling laws could be used to empirically predict crater radius, crater depth, and crater volume; and (4) ascertain if small and intermediate-scale experiments could be used to calibrate our hydrodynamic computer codes.

## EXPERIMENTAL PROCEDURE

The experiment design was similar for both small-scale and intermediate-scale experiments (Fig. 1). In the small-scale experiments, either PETN or RDX explosive was emplaced with a charge length to diameter ratio of 3. These boreholes were stemmed with sand or oil shale fines. Generally, only the depth of burial was varied from experiment to experiment. ANFO or TNT explosives were used in all of the intermediate-scale experiments. Explosive weight and type, charge length, charge diameter, and depth of burial were varied from one experiment to another. Different methods of stemming the shot holes included sand, oil shale fines, gravel, and rock matching grout. The small- and intermediate-scale experiments were sited on the floor or rib of the mine, usually in a location where the surface could be cleaned of debris and dust. Whenever possible, sites were chosen where there was a minimum of blasting damage caused by mining or previous experiments. Photographs of the free surface were taken pre-shot to map any structural flaws that might possibly affect the crater development or the particle size distribution of the resulting rubble. Post-shot photographs of the crater interior were taken to document the character of the oil shale breakage. Volumes of the small-scale craters were determined by measuring the volume of dry sand required to fill the crater. Volumes of the larger craters were calculated from the volume of rubble removed. Depth, long diameter, and short diameter of each crater were also measured (Fig. 1). Rubble from most of the intermediate-scale experiments and 12 small-scale experiments was screened to determine the particle size distribution.

A number of different explosives was used in these cratering tests. All of the explosive weights were normalized to RDX by multiplying by the ratio of the explosive energies (Table 1).

Table 1. Energy of Explosives

| Explosive | Energy (cal/g) |
|---|---|
| RDX | 1480 |
| PETN | 1510 |
| TNT (Prilled) | 1090 |
| ANFO | 1246 |

In order to compare the results of cratering tests that employed significantly different explosives, the charge weights, crater dimensions, and crater volumes were scaled by a function of explosive weight. The four scaled parameters used were:

$$\text{scaled depth of burial (SDOB)} = \frac{\text{depth of burial}}{(\text{charge weight})^{1/3}}$$

$$\text{scaled depth of crater (SDEPC)} = \frac{\text{depth of crater}}{(\text{charge weight})^{1/3}}$$

$$\text{scaled radius of crater (SRAD)} = \frac{\text{average crater radius}}{(\text{charge weight})^{1/3}}$$

$$\text{scaled volume of crater (SVOL)} = \frac{\text{volume of crater}}{\text{charge weight}}$$

The choice of cube-root scaling of crater dimensions is based on the analysis of data from experiments that were performed near optimum scale depth (Fig. 2). Optimum depth is defined as the shallowest depth of burial at which the maximum volume, radius, or depth of crater is observed. Realizing the measurement error of the data and the large variation in crater dimensions and crater volume caused by the site specific geology, we chose to scale the linear crater dimensions by charge weight to the 1/3 power and volume by the charge weight. Analysis of cratering experiments in alluvium at the Nevada Test Site (Ref. 1) shows that for small explosions (less than 1000 lb of TNT) the inherent scatter in the data is sufficient to obscure any deviation from cube-root rules. All of our cratering tests use charge weights significantly lower than 1000 lb of TNT.

During the first few cratering experiments at the Colony Mine it became obvious that the site specific geology was playing a major role in crater formation (Ref. 2). Also, the effect of the site geology varied radically from experiment to experiment. Evaluation of experiment sites and analysis of the post-shot craters required the development of a scheme to quantitatively identify the geologic complexity of each experimental site. After examining several intermediate-scale experiments and several hundred small-scale experiments we chose to use the following classification scheme:

(1) Geologic complexity of 1 indicates that in pre-shot site examination there were few if any identifiable flaws or fractures on the surface in the

immediate vicinity of the experiment. Post-shot craters are essentially symmetrical with no extensive breakage along joints or fractures.

(2) Geologic complexity of 2 indicates that there were a few flaws and fractures on the surface from pre-shot site examination. Pre-existing fractures are generally tight. Post-shot craters are influenced to a minor extent by preexisting flaws and fractures, that is, crater perimeter limited by a fracture or perhaps breakage to a fracture along a bedding plane limited the crater depth.

(3) Geologic complexity of 3 indicates that there were several flaws and fractures in the immediate vicinity of the shot-hole. Some of these fractures may be open. The preexisting geologic structure exerts a major influence on the final shape of the crater. The bottom of the crater may be limited to a single bedding plane fracture. Fractures near the shot-hole may severely restrict crater growth.

(4) Geologic complexity of 4 was assigned to all of the intermediate-scale experiments. Since scaled volumes, scaled radii, and scaled depths of craters were different from those parameters measured in complexity 1, 2, and 3 craters, we inferred that features such as tuff layers, joints, major fractures, vugs, and perhaps changes in grade were affecting crater development and particle size distributions.

The geologic complexity of a particular site is a function of the volume of rock involved in the experiment. For example, an experiment using 5 g of RDX will result in fractures that extend less than 20-50 cm from the shot-hole. The natural joint and fracture spacing at Anvil Points and at Colony is such that many small-scale experiment sites could be located where there were few fractures and joints. However, an intermediate-scale experiment using a charge weight of 10 kg will involve more than 10 $m^3$ of rock and there is no site of that size in Colony or Anvil Points that would be free of joints and fractures. Features at a site that will be important in crater development are those flaws, fractures, and joints that have a size comparable to a crater radius. Features smaller than this may control or affect the particle size distribution but not the crater dimensions.

## FRACTURE PATTERNS

On several of the small-scale experiments, 90 x 90 x 2-cm rubber mats were centered over the explosive borehole to restrict the movement of the fractured rock. Post-shot examination of these craters with the fractured rock in place detail the influence of the pre-shot fractures on the explosive fracturing process. These craters were excavated in layers so that zones of different rock breakage could be identified and mapped.

The typical surface fracture pattern of complexity 1 craters (Fig. 3) include well-developed radial fractures originating at the explosive borehole and well defined concentric cracking centered around the borehole. The largest pieces of rubble are near the crater perimeter and the fines are restricted to a small volume near the charge. The crater perimeter is defined by a set of concentric cracks.

The typical surface fracture pattern of complexity 2 craters (Fig. 4) exhibits poorly developed radial fractures that are captured by the first pre-existing fractures encountered. The concentric cracking is almost

completely masked by cracking along pre-existing joints. With the exception of a small volume of fines in the immediate vicinity of the charge, the rock breakage is controlled by the spacing of the pre-shot fracture system with large pieces of rubble formed where the fracture spacing is largest. The perimeter of this asymmetrical crater is elongated along the strike of the natural fracture system.

The fracture pattern observed in a typical complexity 3 crater (Fig. 5) is an exaggerated version of the complexity 2 fractures with no system of radial or concentric fractures obvious. Fines are restricted to the immediate vicinity of the borehole and the size of larger pieces of rubble is controlled by natural fracture spacing. The perimeter of the crater is defined entirely by straight line segments where rock has broken along pre-existing fractures.

Complexity 4 craters exhibit fracture patterns that are very similar to patterns observed in complexity 2 craters, that is, some radial fractures developed but were usually captured by the pre-existing joint system. Occasionally fracture patterns similar to complexity 3 patterns develop when major joints are present.

## CRATER PROFILES

Fifteen of the small-scale craters were profiled to examine the effects of fractures and weak bedding planes on the shape of explosively formed craters in oil shale (Fig. 6). Craters in a simple geologic setting (complexity = 1) have relatively smooth contours with the crater walls composed of equal-length, angular breaks and bedding plane fractures that give the crater profile a somewhat terraced appearing side. The crater size is controlled by the design criteria (charge size, depth of burial, etc.). When experiments were duplicated, the crater measurements were reproducible to 10-15%.

Craters in slightly more complex geologic setting (complexity = 2) also have relatively smooth contours with profiles having terraced sides similar to complexity 1 craters, but the length of the angular breaks are no longer equal to the breaks along the bedding planes. The overall appearance of the complexity 2 craters is more angular than the complexity 1 craters. These experiments were not as reproducible as the complexity 1 sites, with crater measurements varying 15-20% from experiment to experiment.

Complexity 3 profiles are predominately steep sided with large areas broken along the bedding planes. The craters are usually very asymmetric with the pre-existing fractures controlling the crater size and shape. In some cases, these fractures allow craters to develop to depths below the bottom of the explosive charge. Crater dimensions varied more than 50% between identically designed experiments at different sites.

Average crater profiles for complexity 1 experiments (Fig. 7) show an increase in radius and depth with scaled depth of burial until the optimum depth is reached, then a decrease in radius and depth until critical depth is reached. Critical depth is defined as the shallowest depth of burial at which failure of the rock does not occur at the surface. The slope of the sides of these craters is greater near the optimum crater depth and then flattens to a more dish-like crater as the scaled depth of burial approaches the surface or near critical depth. The average crater profiles for complexity 2 experiments show an increase in depth and radius with scaled depth of burial. No profile data are available for scaled depths below optimum scaled depth. The craters

of experiments with a geologic complexity of 3 are significantly more irregular. While the crater depth and radius generally increase with depth of burial until optimum depth is reached, individual experiments vary considerably.

Profiles of intermediate-scale cratering experiments at both the Colony and Anvil Points mines show many features that are similar to features observed in the small-scale experiments (Ref. 3). Joints and major fractures control the extent of intermediate-scale craters in the same manner that large flaws and fractures control the extent of small-scale craters. Terracing also occurs along major bedding plane fractures, but not to the relative extent that it does in complexity 3 craters.

A number of intermediate-scale experiments were done at a scale depth of burial of approximately 9.0 $cm/g^{1/3}$. Crater profiles for these show a large variation in crater radius and crater depth; craters that have similar experiment design (for example, Experiments 3 and 6 with scaled depths of burial of 9.3 and 9.2, respectively, and explosive weights of 21.6 kg and 22.2, respectively) vary in depth by 30% and in radius by 100%. A comparison of the north-south and east-west profiles in Experiment 4 (Fig. 8) shows a large variation in the same crater depending on whether the profiles are run parallel to the strike or direction of the joint and fracture system, or perpendicular to it. The single borehole intermediate-scale craters are usually elongated in the direction of the prominent joint or fracture system.

There is one major difference between the small- and intermediate-scale craters. The intermediate-scale craters have steeper sides near the charge and then the sides flatten out toward the rim of the crater, whereas the small-scale craters tend to be shallow cones. When only the rock that has been broken and tumbled is removed from an intermediate-scale crater, the crater profile is very similar to small-scale craters.

## PARTICLE SIZE DISTRIBUTIONS

Rubble from 12 small-scale experiments was screened to provide particle-size distributions for sites with different geologic complexities (Table 2). The particle-size distribution for small-scale experiments changes substantially with the geologic complexity of each particular experiment site (Fig. 9). At those sites where there are few pre-shot fractures, 50% of the rubble is 0-2.0 cm. At those sites where fractures played some role in the shape of the craters (geologic complexity = 2), 50% of the rubble is 0-3.1 cm. At those sites where there were several fractures existing pre-shot (geologic complexity = 3), 50% of the rubble is 0-5.7 cm with a significant percentage of material being greater than 7.6 cm.

The particle-size distribution for these experiments appears to be a direct function of the complexity of the pre-shot site geology, that is, the number of flaws and fractures. With this in mind, the screening data on intermediate-scale experiments at the Colony (Ref. 4) and Anvil Points mines were reexamined (Fig. 10, Table 3).

The curve for Experiment No. 4 is offset upward because of the measurement of fines (less than 5.5 cm). When this crater was excavated and the associated flyrock was picked up, fines that covered the floor to a depth of 30 cm pre-shot were unavoidably scooped up by the front loader. Because of this problem on Experiment No. 4 and similar but less severe problems at other Colony Mine experiment sites, the fines (less than 5) measurements should be

Table 2. Particle Size Distribution for Small-Scale Experiments

| Experiment No. | GC[a] | Percentage of Rock for Each Screen Size | | | | | |
|---|---|---|---|---|---|---|---|
| | | 0-.6 (cm) | .6-1.2 (cm) | 1.2-2.5 (cm) | 2.5-5.1 (cm) | 5.1-7.6 (cm) | 7.6-10.1 (cm) |
| 30 | 1 | 9.5 | 21.6 | 38.0 | 20.7 | 10.2 | 0 |
| 42 | 1 | 6.3 | 18.4 | 37.3 | 29.3 | 8.7 | 0 |
| 44 | 2 | 4.8 | 12.7 | 27.8 | 26.5 | 17.2 | 11.0 |
| 76 | 2 | 4.1 | 13.0 | 42.9 | 26.5 | 9.9 | 3.6 |
| 99 | 2 | 4.7 | 6.3 | 32.2 | 14.1 | 20.6 | 22.1 |
| 102 | 2 | 2.8 | 6.8 | 18.9 | 43.5 | 28.0 | 0 |
| 166 | 2 | 4.6 | 7.6 | 20.9 | 31.6 | 31.9 | 3.4 |
| 46 | 3 | 3.2 | 8.8 | 21.0 | 17.1 | 15.2 | 34.7 |
| 139 | 3 | 2.1 | 6.9 | 12.3 | 36.2 | 19.6 | 22.9 |
| 147 | 3 | 1.3 | 0.9 | 12.3 | 23.8 | 25.9 | 35.8 |
| 149 | 3 | 0.4 | 1.1 | 0.9 | 11.4 | 27.7 | 58.5 |
| 150 | 3 | 1.3 | 4.7 | 18.4 | 32.8 | 42.8 | 0 |
| Average | 1 | 7.9 | 20.0 | 37.7 | 25.0 | 9.4 | 0 |
| Average | 2 | 4.2 | 9.3 | 28.5 | 28.5 | 21.5 | 8.0 |
| Average | 3 | 1.7 | 4.4 | 13.0 | 24.2 | 26.3 | 30.4 |

[a] Geologic Complexity (GC)

Table 3. Particle-Size Distribution for Intermediate-Scale Experiments (Complexity 4)

| Experiment No. | Percentage of Rock by Weight for Each Screening Interval | | | | | | | |
|---|---|---|---|---|---|---|---|---|
| | 0-5.1 (cm) | 5.1-10 (cm) | 10-15 (cm) | 15-20 (cm) | 20-30 (cm) | 30-46 (cm) | 46-61 (cm) | >61 (cm) |
| 1 | 33 | 24 | 13 | ---- 22 ---- | | --------- 8 --------- | | |
| 2 | 31 | 29 | 14 | ---- 21 ---- | | --------- 5 --------- | | |
| 3 | 18 | 20 | 11 | ---- 25 ---- | | -------- 26 --------- | | |
| 4 | 41 | 9 | 5 | 7 | 9 | 11 | ---- 18 ---- | |
| 5 | 38 | 19 | 13 | ---- 22 ---- | | -------- 8 --------- | | |
| 6 | 19 | 18 | 14 | ---- 22 ---- | | -------- 27 --------- | | |
| 7 | ------- 21 ------- | | | ---- 23 ---- | | 16 | 22 | 18 |
| 8 | 16 | 9 | 3 | ---- 12 ---- | | 10 | 9 | 40 |
| 10 | 18 | 11 | 10 | ---- 7 ---- | | 5 | 16 | 33 |

viewed with some suspicion. Three distinct groups of curves can be seen in Figure 11: (1) the Colony mine particle-size distributions group together; (2) experiments 3 and 6 at Anvil Points group together; and (3) experiments 1, 2, and 5 at Anvil Points group together. The mean particle size is 25 cm in the Colony experiments, 11 cm in experiments 3 and 6, and 6 cm in experiments 1, 2, and 5.

Although the larger pieces of rubble in each experiment are lumped together in the last screening interval, there were systematic differences between experiments at Colony and Anvil Points. The largest pieces of rubble at Colony were 1 to 2 m on a side, whereas, at Anvil Points few pieces of rubble were as large as 1 m.

A preliminary analysis of the pre-shot fracture maps in both Colony and Anvil Points shows significantly different fracture distributions. The mean fracture spacing (measured perpendicular to the strike of the fracture system) is about 80 cm at Colony, about 35 cm at the experiment 3 and 6 sites at Anvil Points, and about 20 cm at the experiment 2 site at Anvil Points. Curiously, the resultant mean particle size appears to be about one-third the mean fracture spacing at each site. In these intermediate-scale experiments, the particle-size distribution is only a function of the complexity of the geologic setting, thus behaving similarly to the small-scale experiments.

Changing the engineering parameters (depth, diameter, charge weight, etc.) had little effect on the particle size distribution of single borehole cratering experiments shot to an infinite free face.

## SCALING PARAMETERS

The examination of the crater profiles and the particle-size distributions from the various small- and intermediate-scale experiments indicates that the site geology, that is, flaws, fractures and joints, have a pronounced, if not overwhelming, effect on final shape and size of the crater. Using cube-root scaling, the average crater radius, crater depth, and crater volume (Tables 4 and 5) were examined in detail to determine optimum and critical depths.

It is apparent from plots of scaled volume vs scaled depth of burial (Figs. 11 and 14) that the critical depths for each geologic complexity are substantially different. (Note: The numbers with each bar in Figures 12-14 are the number of data points averaged to produce the bar.) The shape of the four curves is similar, with the optimum (or maximum) values skewed to the right at 0.7 of critical depth. The curves are quite similar in shape to cratering curves determined for single borehole experiments in alluvium at the Nevada Test Site (Ref. 5).

The optimum scaled crater radius (Figs. 12 and 14) varies from 10 $cm/g^{1/3}$ in the simple geology to 16 $cm/g^{1/3}$ in the most complex geology. The scaling curves for crater depth have shape similar to both the volume and radius curves (Figs. 13 and 14). The optimum scaled crater depth varies from 3.5 $cm/g^{1/3}$ in the complexity 1 sites to 12 $cm/g^{1/3}$ in the complexity 4 sites.

The optimum values of volume and radius for intermediate-scale experiments are somewhat higher than for the complexity 3 curves, but there is a factor of two difference in optimum crater depth (Table 6). This apparent discrepancy is a function of the scaling exponent used. The crater depths did

Table 4. Small-Scale Experiment Cratering Data

| SDOB Range | Geologic Index = 1 | | | | | | Geologic Index = 2 | | | | | | Geologic Index = 3 | | | | | |
|---|---|---|---|---|---|---|---|---|---|---|---|---|---|---|---|---|---|---|
| | SVOL. | No. | SRAD | No. | SDEPC | No. | SVOL. | No. | SRAD | No. | SDEPC | No. | SVOL. | No. | SRAD | No. | SDEPC | No. |
| 0 - 1 | - | (0) | - | (0) | - | (0) | 63.6 | (1) | 1.31 | (1) | 1.31 | (1) | - | (0) | - | (0) | - | (0) |
| 1 - 2 | 100 | (4) | 6.31 | (5) | 1.75 | (5) | 198 | (4) | 7.40 | (4) | 2.00 | (4) | 214 | (5) | 6.80 | (4) | 2.17 | (5) |
| 2 - 3 | 215 | (2) | 7.69 | (2) | 2.66 | (2) | 474 | (2) | 11.9 | (2) | 2.30 | (2) | 496 | (3) | 8.83 | (6) | 2.59 | (6) |
| 3 - 4 | 322 | (5) | 8.37 | (6) | 3.45 | (6) | 540 | (3) | 8.32 | (6) | 2.84 | (6) | 595 | (5) | 9.96 | (6) | 3.99 | (6) |
| 4 - 5 | 370 | (2) | 8.58 | (2) | 2.81 | (2) | 414 | (1) | 8.82 | (3) | 3.10 | (3) | 780 | (7) | 11.85 | (7) | 3.51 | (8) |
| 5 - 6 | 325 | (4) | 8.64 | (4) | 2.69 | (4) | 352 | (3) | 8.23 | (4) | 3.00 | (4) | 636 | (10) | 9.56 | (16) | 3.74 | (16) |
| 6 - 7 | 489 | (4) | 10.4 | (4) | 2.38 | (4) | 721 | (4) | 9.72 | (7) | 3.28 | (7) | 1040 | (11) | 12.21 | (13) | 4.28 | (13) |
| 7 - 8 | 496 | (8) | 8.39 | (6) | 2.20 | (6) | 815 | (6) | 10.6 | (5) | 2.96 | (5) | 765 | (10) | 10.6 | (15) | 4.03 | (15) |
| 8 - 9 | 54.2 | (3) | 3.37 | (3) | 0.99 | (3) | 731 | (3) | 11.2 | (3) | 4.38 | (3) | 988 | (8) | 13.6 | (12) | 4.33 | (12) |
| 9 - 10 | 0 | (3) | 0 | (3) | 0 | (3) | 585 | (3) | 7.34 | (4) | 3.22 | (4) | 1616 | (12) | 10.9 | (13) | 4.19 | (13) |
| 10 - 11 | 0 | (4) | 0 | (4) | 0 | (4) | 54.6 | (4) | 4.00 | (5) | 0.88 | (5) | 1369 | (6) | 12.2 | (7) | 5.99 | (7) |
| 11 - 12 | - | | - | | - | | 0 | (2) | 0 | (2) | 0 | (2) | 695 | (2) | 8.84 | (3) | 4.75 | (3) |
| 12 - 13 | - | | - | | - | | 0 | (3) | 0 | (3) | 0 | (3) | 372 | (4) | 9.69 | (4) | 3.13 | (4) |
| 13 - 14 | - | | - | | - | | 0 | (2) | 0 | (2) | 0 | (2) | 101 | (6) | 2.61 | (6) | 0.69 | (6) |
| 14 - 15 | - | | - | | - | | 0 | (2) | 0 | (2) | 0 | (2) | 87.6 | (8) | 1.85 | (8) | 0.95 | (8) |
| 15 - 16 | - | | - | | - | | - | | - | | - | | 111 | (7) | 1.93 | (7) | 0.44 | (7) |
| 16 - 17 | - | | - | | - | | - | | - | | - | | 0 | (4) | 0 | (4) | 0 | (4) |
| 17 - 18 | - | | - | | - | | - | | - | | - | | 158 | (6) | 3.46 | (6) | 1.02 | (6) |
| 18 - 19 | - | | - | | - | | - | | - | | - | | 12.1 | (6) | 0.59 | (6) | 0.22 | (6) |
| 19 - 20 | - | | - | | - | | - | | - | | - | | 0 | (3) | 0 | (3) | 0 | (3) |
| 20 - 21 | - | | - | | - | | - | | - | | - | | 0 | (2) | 0 | (2) | 0 | (2) |
| 21 - 22 | - | | - | | - | | - | | - | | - | | 0 | (1) | 0 | (1) | 0 | (1) |
| 22 - 23 | - | | - | | - | | - | | - | | - | | 0 | (2) | 0 | (2) | 0 | (2) |

Table 5. Intermediate-Scale Experiment Cratering Data

| Experiment Number | Weight of Explosive (kg)[a] | Scaled Depth of Burial | Scaled Volume | Scaled Radius | Scaled Depth of Crater | Symmetry | Aspect Ratio |
|---|---|---|---|---|---|---|---|
| 1 | 24.9* | 8.33 | 201 | 7.74 | 10.0 | --- | 1.30 |
| 2 | 24.4* | 8.92 | 1150 | 11.7 | 11.4 | .79 | .97 |
| 3 | 21.6* | 9.26 | 1130 | 15.2 | 9.52 | .51 | .63 |
| 4 | 20.8 | 8.86 | 823 | 15.0 | 9.13 | .95 | .61 |
| 5 | 29.4 | 9.43 | 635 | 12.4 | 8.0 | .87 | .64 |
| 6 | 22.2 | 9.18 | 1060 | 15.5 | 11.0 | .91 | .71 |
| 7 | 4.39 | 10.1 | 1270 | 12.7 | 8.24 | .91 | .65 |
| 8 | 8.13 | 11.4 | 1320 | 12.9 | 9.94 | .62 | .80 |
| 9 | 12.2 | 11.8 | 1280 | 16.2 | 11.3 | .71 | .70 |
| 10 | 12.2 | 12.2 | 410 | 9.77 | 5.21 | .50 | .53 |
| 11 | 4.39 | 13.7 | 1480 | 12.4 | 11.0 | .76 | .89 |
| 12 | 4.39 | 13.8 | 1560 | 14.6 | 12.2 | .57 | .83 |
| 13 | 76.4 | 13.9 | 0 | No Crater | 0 | | |
| 14 | 76.4 | 14.3 | 773 | 11.7 | 9.43 | .66 | .81 |
| 15 | 12.2 | 17.7 | 0 | No Crater | 0 | | |
| 16 | 4.39 | 21.1 | 0 | No Crater | 0 | | |

[a] All explosives normalized to RDX.

* Explosive is ANFO except for (*) experiments that used prilled TNT.

Table 6. Optimum and Critical Scaling Parameters

| | Geologic Complexity | | | |
|---|---|---|---|---|
| | 1 | 2 | 3 | 4 |
| Critical Scaled Depth of Burial ($cm/g^{1/3}$) | 9 | 11 | 16 | 18 |
| Scaled Volume | | | | |
| Optimum Depth of Burial ($cm/g^{1/3}$) | 7 | 7.5 | 9.5 | 14 |
| Optimum Volume ($cm^3/g$) | 500 | 800 | 1600 | 1500 |
| Scaled Radius | | | | |
| Optimum Depth of Burial ($cm/g^{1/3}$) | 6.5 | 8.5 | 10.5 | 11.5 |
| Optimum Radius ($cm/g^{1/3}$) | 10 | 11 | 12 | 16 |
| Scaled Depth of Crater | | | | |
| Optimum Depth of Burial ($cm/g^{1/3}$) | 3.5 | 8.5 | 10.5 | 12 |
| Optimum Depth of Crater ($cm/g^{1/3}$) | 3.5 | 4.4 | 6.0 | 12 |

not scale as $w^{1/3}$ at small charge sizes; they scale closer to $w^{0.4}$. The $w^{1/3}$ scaling is probably appropriate to the intermediate-scale experiments and the deviation from this at small charge sizes is due to preferential fracture along a few shallow bedding planes common to all of the experiment sites.

To quantify the shape of the crater, two additional parameters, symmetry and aspect ratio, were calculated from the measured crater dimensions. Symmetry is defined as the ratio of the short diameter to the long diameter and aspect ratio is defined as the depth of the crater divided by the average crater radius. Symmetry vs aspect ratio was plotted (Fig. 15) to determine if there were systematic differences in crater shape associated with geologic complexity. Each geologic complexity is different with the complexity 2 experiments plotting as a subset of complexity 3, and complexity 1 experiments plotting as a subset of complexity 2 experiments. Although the data set is small, the complexity 4 experiments plot separately with overlap into complexity 2 and 3 zones.

## CONCLUSIONS

Site specific geology plays a major role in the final shape of a crater. Sites with a minimum of flaws and fractures (pre-shot) are symmetrical and reproducible from experiment to experiment. Sites with complex pre-shot flaw distributions tend to be asymmetric and the character of the craters varies substantially from experiment to experiment.

Particle size distributions for simple cratering experiments using charge weights from a few grams to 100 kg appear to be almost totally controlled by the pre-shot geology, that is, the distribution of flaws, joints, and fractures. The use of cratering experiments to a free face to evaluate the effect on particle size distribution by explosive type, explosive geometry, or depth of burial of the charge appears to be futile. Only the breakage in the immediate vicinity of the charge changes and most of the rock is broken along pre-existing flaws. The difference in particle size distribution between single borehole intermediate-scale cratering experiments at Colony and Anvil

Points is due only to the inherent difference in the pre-shot site flaw distributions at these two mines. Experiments designed to alter the "normal" particle size distribution must utilize multiple boreholes, limited free face, or presplitting to bound the experiment so that the volume of rock acted upon by the explosive is small compared to a cratering experiment shot to an infinite free face.

Scaling laws developed from small- and intermediate-scale cratering experiments at the Colony and Anvil Points mines can be used to quantitatively predict crater volumes, average radius, and depth. The geologic complexity of each experiment site has a major effect on the scaling parameters, with experiments in simple sites having smaller critical and optimum depths of burial. As the geologic complexity increases, generally the volume, crater depth, and average crater radius increases.

Since any individual experiment may differ substantially from a "typical experiment" at a particular scaled depth of burial, substantial error may result if an individual experiment or a few experiments are used to prove or verify a computer hydrocode. The fact that measurements of volume, radius, or crater depth made on a specific experiment either agree or disagree could be coincidental and not reflect on the accuracy of the hydrodynamic computer code results. Statistical averages of many experiments would provide far more representative parameters to compare to hydrocode results. Clearly, the phenomenology of an explosive cratering experiment is overwhelmingly controlled by the pre-existing flaw distribution. Until this flaw distribution is incorporated in detail in the models, accurate hydrodynamic computer code predictions of crater volumes, radii, depths, profiles, and particle size distributions for an individual experiment cannot be accomplished. However, it is possible that some parameters such as particle velocity and surface accelerations and velocities may be accurately modeled without incorporating the detailed geology (Ref. 6).

## ACKNOWLEDGMENTS

The work reported here was performed under U.S. Department of Energy Contract No. W-7405-ENG 36. The authors also wish to express their appreciation to the personnel of the Atlantic Richfield Company at Colony Mine and the personnel of Science Applications, Inc., at Anvil Points Mine for their assistance with these experiments.

REFERENCES

1. Chabai, A. J., On Scaling Dimensions of Craters Produced by Buried Explosives, Journal of Geophysical Research, Vol. 70, No. 20, 1965

2. Ray, J. M., Harper, M. D., Craig, J. L., and Edwards, C. L., Influence of Site-Specific Geology on Oil Shale Fragmentation Experiments at the Colony Mine, Garfield County, Colorado, LA-UR-82-1852, Los Alamos National Laboratory, 1982

3. Harper, M. D., and Ray, J. M., Experimental Design and Crater Profiles of Intermediate Scale Experiments in Oil Shale, LA-8553-PR, Los Alamos National Laboratory, 1980

4. Harper, M. D., and Oliver, R. D., Data from the Screening of the Rubble from Eight Cratering Experiments in Oil Shale, LA-8732-MS, Los Alamos National Laboratory, 1981

5. Carlson, R. H., Crater Scaling as a Function of Charge Burst Depth, SC-CR-72 3177, Sandia National Laboratories, 1970

6. Margolin, L. G., and Adams, R. F., Numerical Simulation of Fracture, Proceedings, Society of Mining Engineers, AIME, 1982

Illustrations

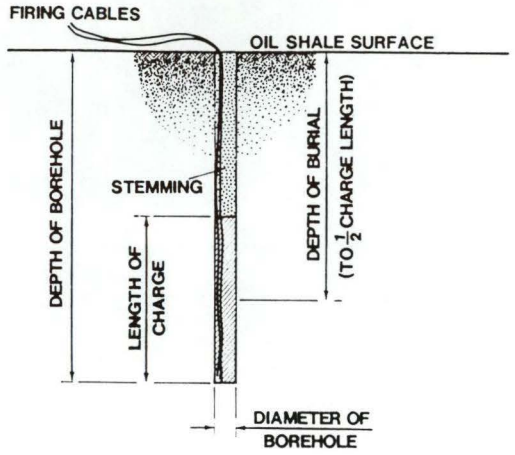
FIRING CABLES
OIL SHALE SURFACE
DEPTH OF BOREHOLE
STEMMING
LENGTH OF CHARGE
DEPTH OF BURIAL (TO ½ CHARGE LENGTH)
DIAMETER OF BOREHOLE

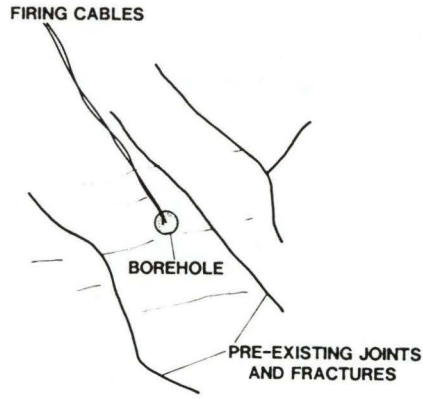
FIRING CABLES
BOREHOLE
PRE-EXISTING JOINTS AND FRACTURES

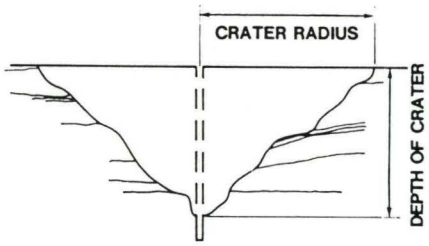
CRATER RADIUS
DEPTH OF CRATER

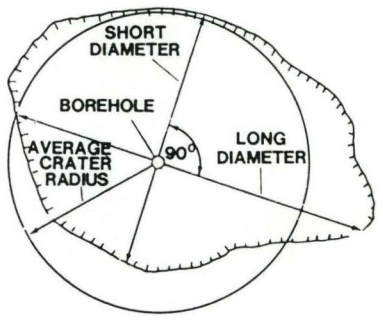
SHORT DIAMETER
BOREHOLE
AVERAGE CRATER RADIUS
90°
LONG DIAMETER

Fig. 1

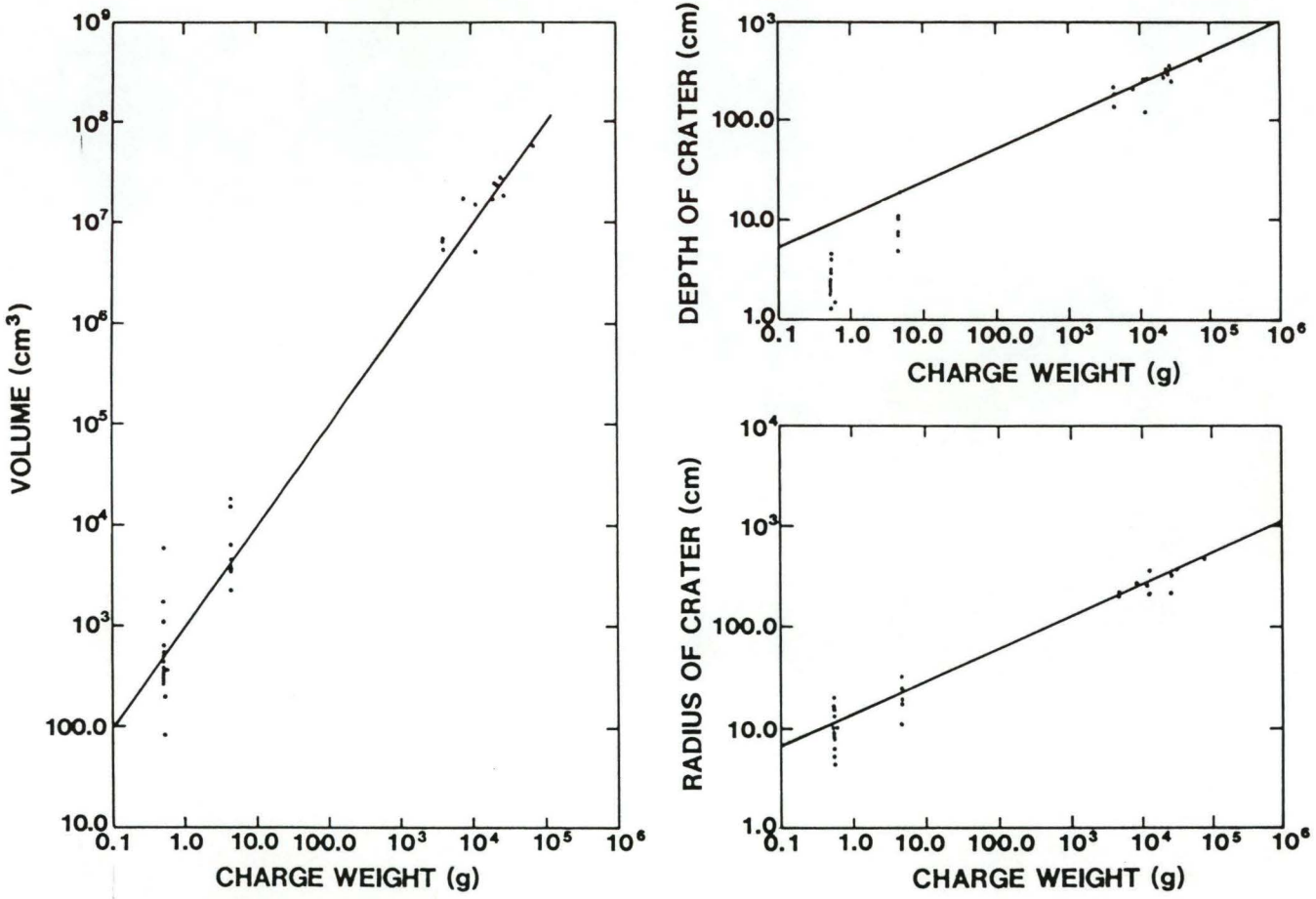
VOLUME (cm³)
10⁹
10⁸
10⁷
10⁶
10⁵
10⁴
10³
100.0
10.0
0.1
1.0
10.0
100.0
10³
10⁴
10⁵
10⁶
CHARGE WEIGHT (g)
DEPTH OF CRATER (cm)
10³
100.0
10.0
1.0
CHARGE WEIGHT (g)
RADIUS OF CRATER (cm)
10⁴
10³
100.0
10.0
1.0
CHARGE WEIGHT (g)

Fig. 2

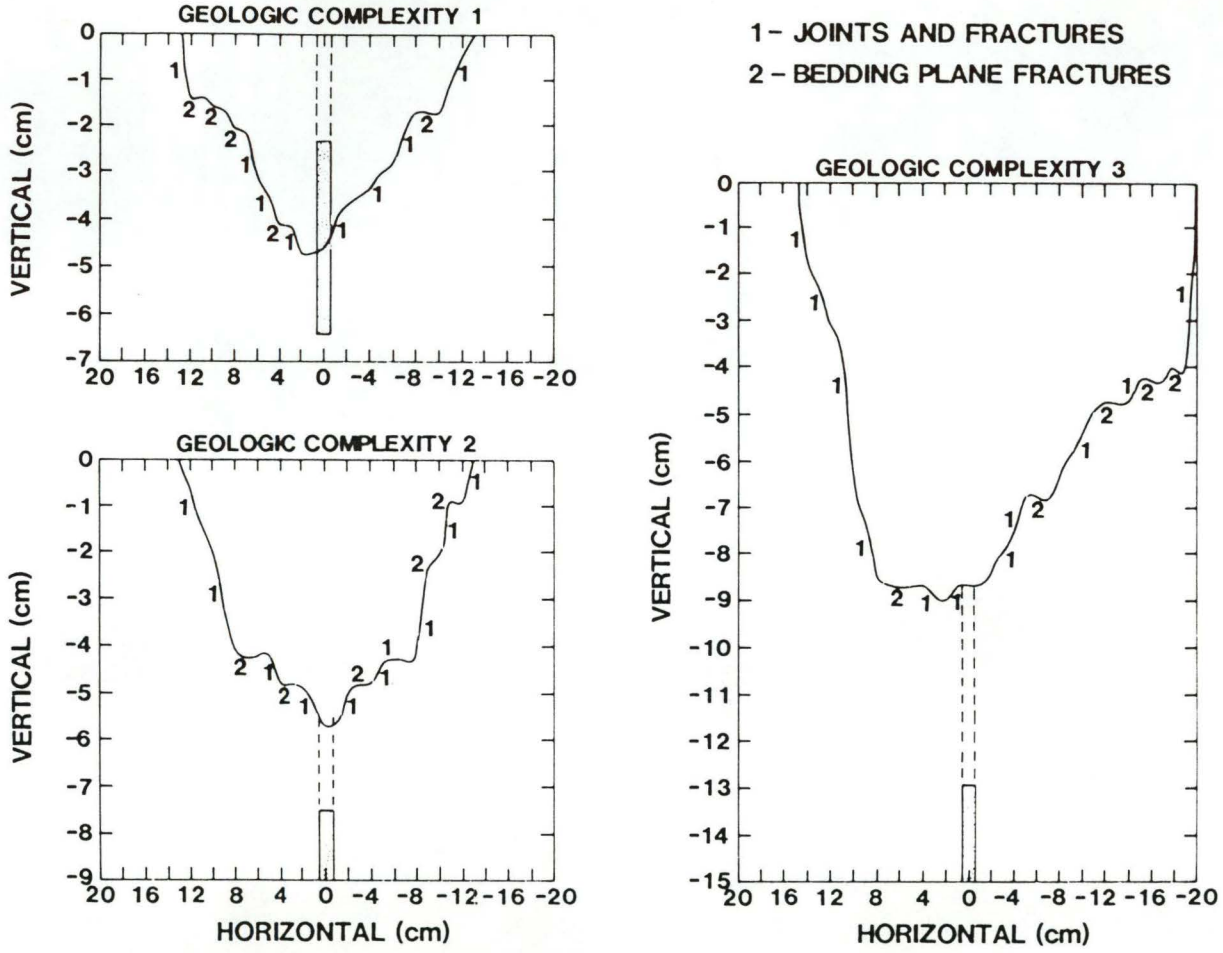
GEOLOGIC COMPLEXITY 1
GEOLOGIC COMPLEXITY 2
GEOLOGIC COMPLEXITY 3
1 – JOINTS AND FRACTURES
2 – BEDDING PLANE FRACTURES
VERTICAL (cm)
HORIZONTAL (cm)
0 -1 -2 -3 -4 -5 -6 -7 -8 -9 -10 -11 -12 -13 -14 -15
20 16 12 8 4 0 -4 -8 -12 -16 -20

Fig. 6

Fig. 1

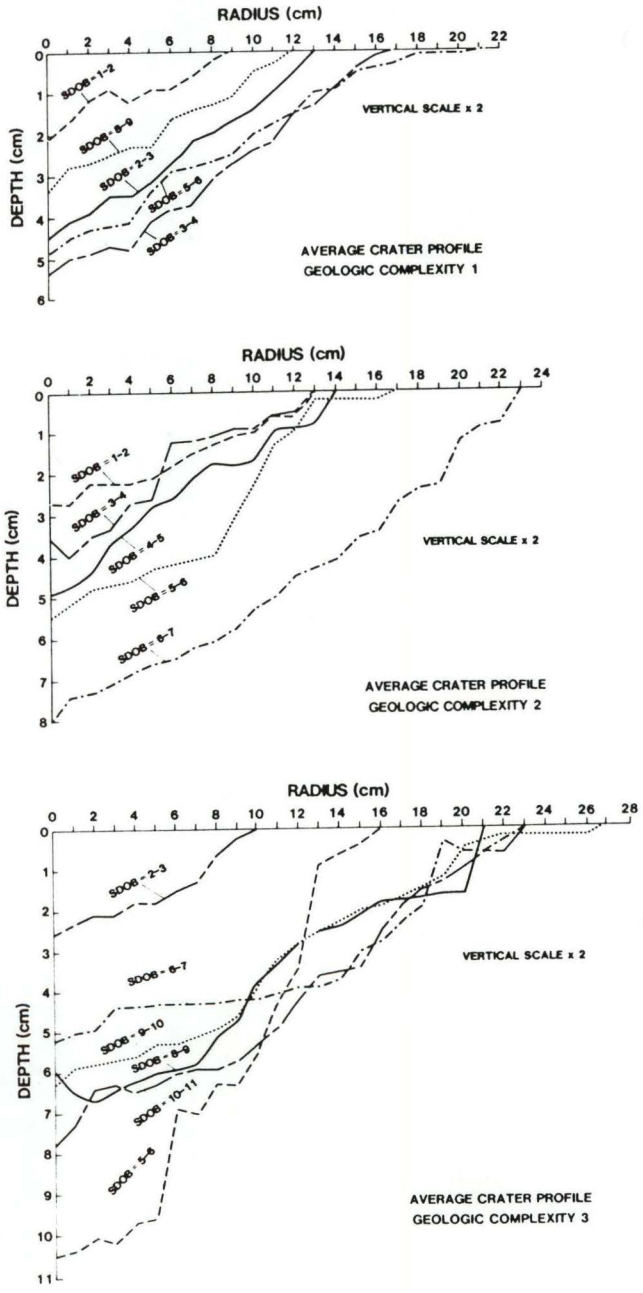
RADIUS (cm)
DEPTH (cm)
SDOS = 1-2
SDOS = 8-9
SDOS = 2-3
SDOS = 5-6
SDOS = 3-4
VERTICAL SCALE x 2
AVERAGE CRATER PROFILE
GEOLOGIC COMPLEXITY 1
RADIUS (cm)
DEPTH (cm)
SDOS = 1-2
SDOS = 3-4
SDOS = 4-5
SDOS = 5-6
SDOS = 6-7
VERTICAL SCALE x 2
AVERAGE CRATER PROFILE
GEOLOGIC COMPLEXITY 2
RADIUS (cm)
DEPTH (cm)
SDOS = 2-3
SDOS = 6-7
SDOS = 9-10
SDOS = 8-9
SDOS = 10-11
SDOS = 5-6
VERTICAL SCALE x 2
AVERAGE CRATER PROFILE
GEOLOGIC COMPLEXITY 3

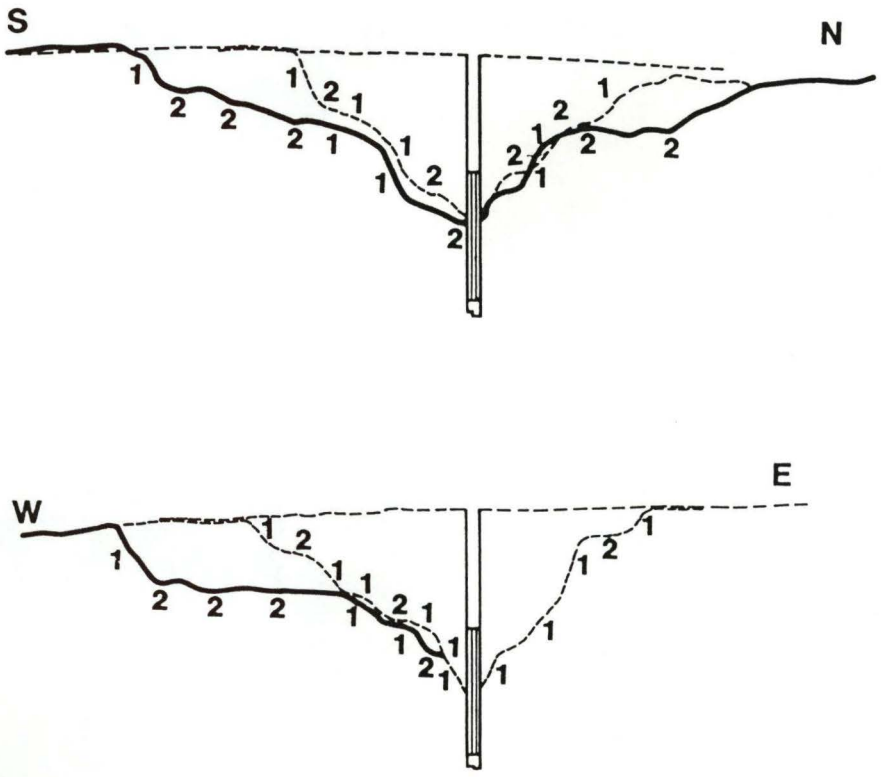
S
N
W
E
0 1 2
METERS
1- JOINTS AND FRACTURES
2- BEDDING PLANE FRACTURES
TUMBLED ROCK
BROKEN ROCK (IN PLACE)

Fig. 9

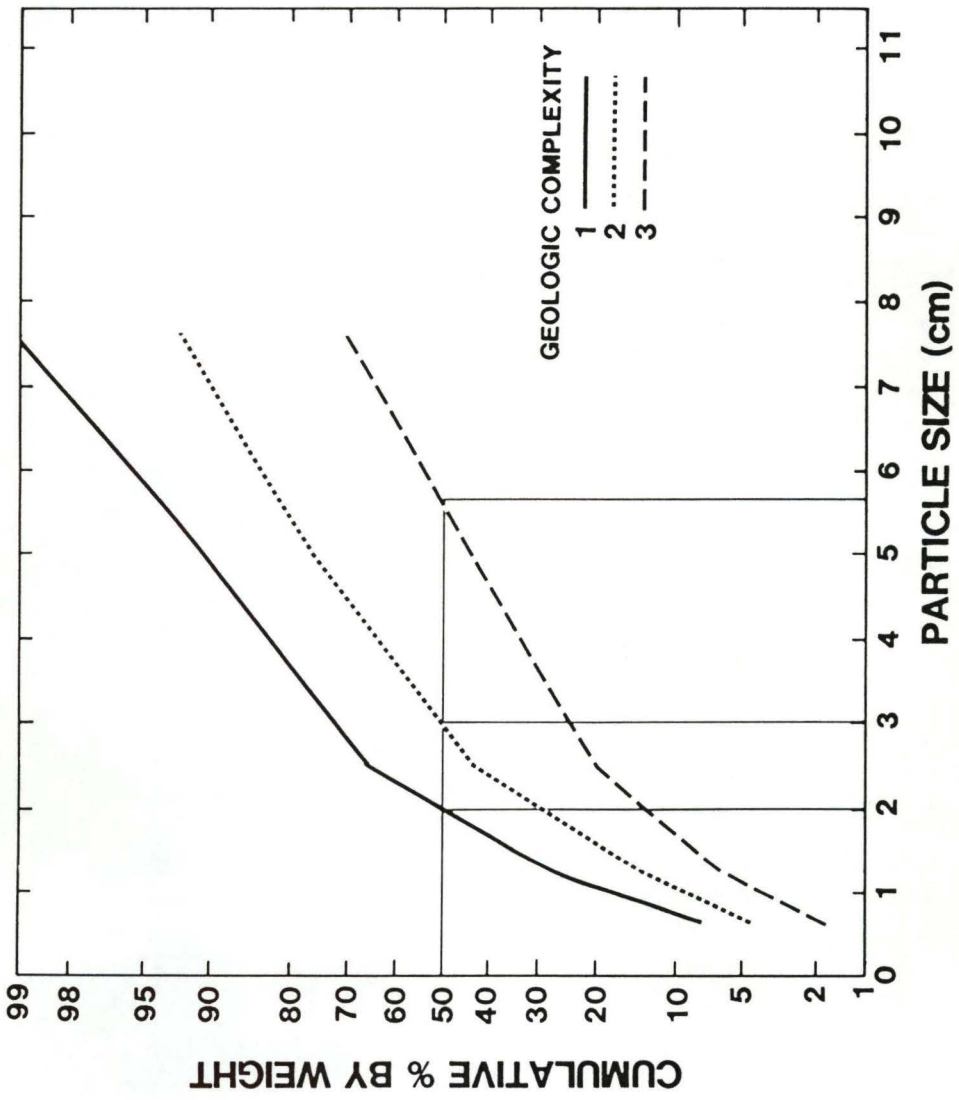
GEOLOGIC COMPLEXITY
1
2
3
CUMULATIVE % BY WEIGHT
99
98
95
90
80
70
60
50
40
30
20
10
5
2
1
0
1
2
3
4
5
6
7
8
9
10
11
PARTICLE SIZE (cm)

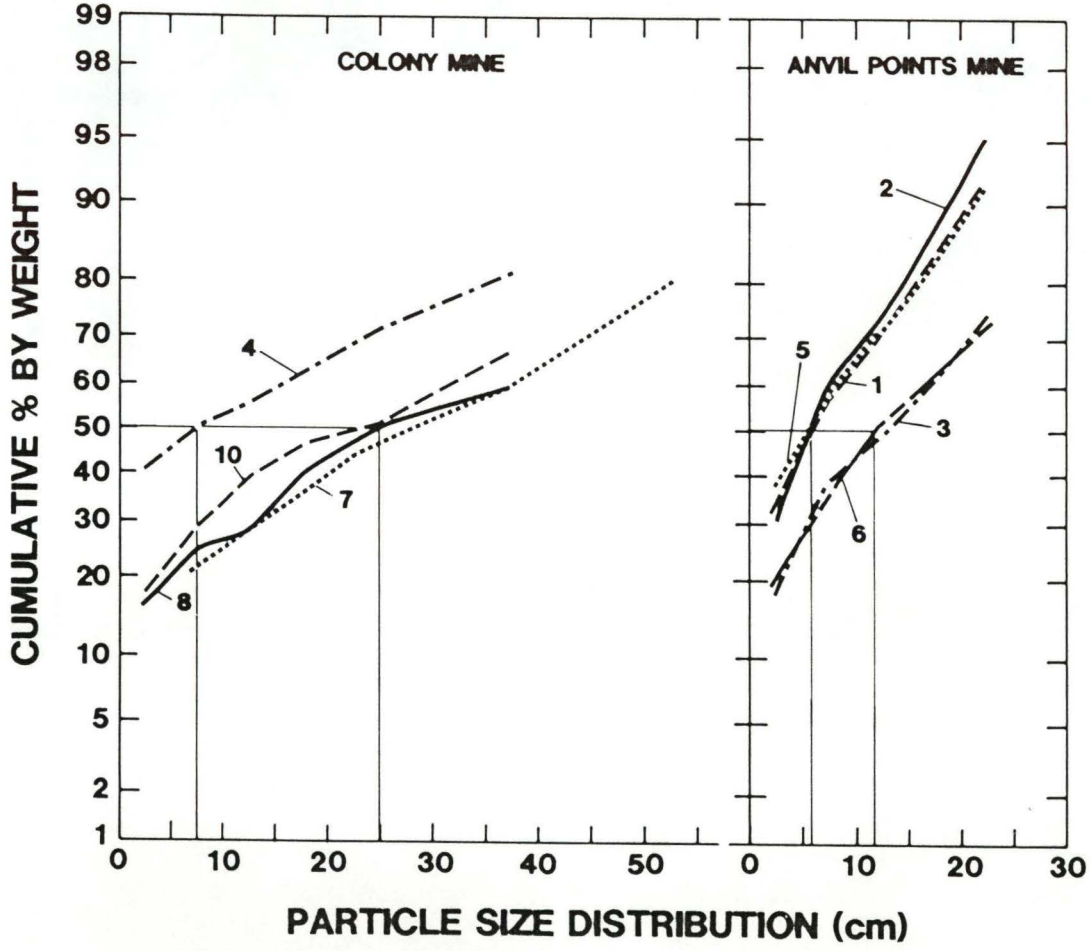
COLONY MINE
ANVIL POINTS MINE
CUMULATIVE % BY WEIGHT
99
98
95
90
80
70
60
50
40
30
20
10
5
2
1
0
10
20
30
40
50
0
10
20
30
1
2
3
4
5
6
7
8
10
PARTICLE SIZE DISTRIBUTION (cm)

Fig. 10

Fig. 11

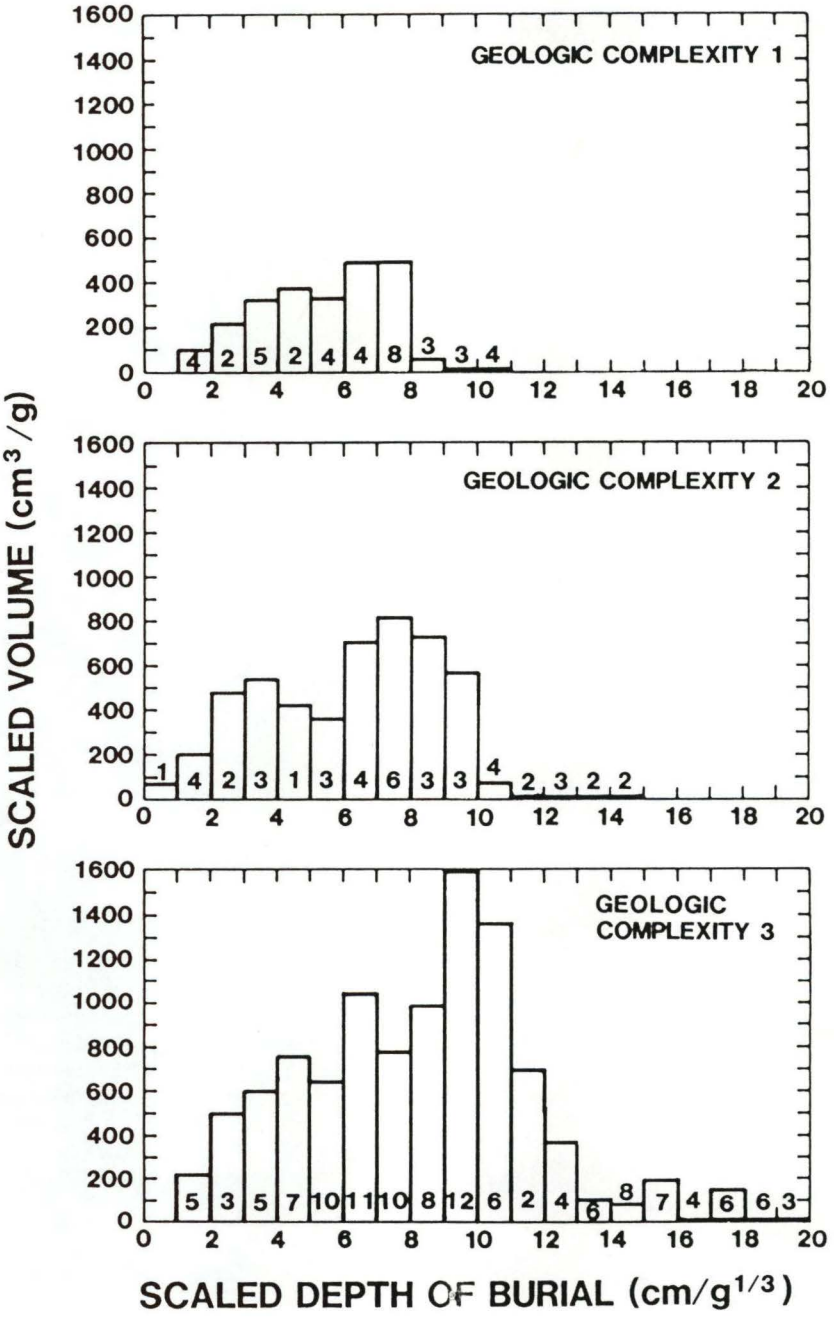
GEOLOGIC COMPLEXITY 1
GEOLOGIC COMPLEXITY 2
GEOLOGIC COMPLEXITY 3
SCALED VOLUME (cm³/g)
SCALED DEPTH OF BURIAL (cm/g^1/3)
0
200
400
600
800
1000
1200
1400
1600
0 2 4 6 8 10 12 14 16 18 20
4 2 5 2 4 4 8 3 3 4
1 4 2 3 1 3 4 6 3 3 4 2 3 2 2
5 3 5 7 10 11 10 8 12 6 2 4 6 8 7 4 6 6 3

Fig. 12

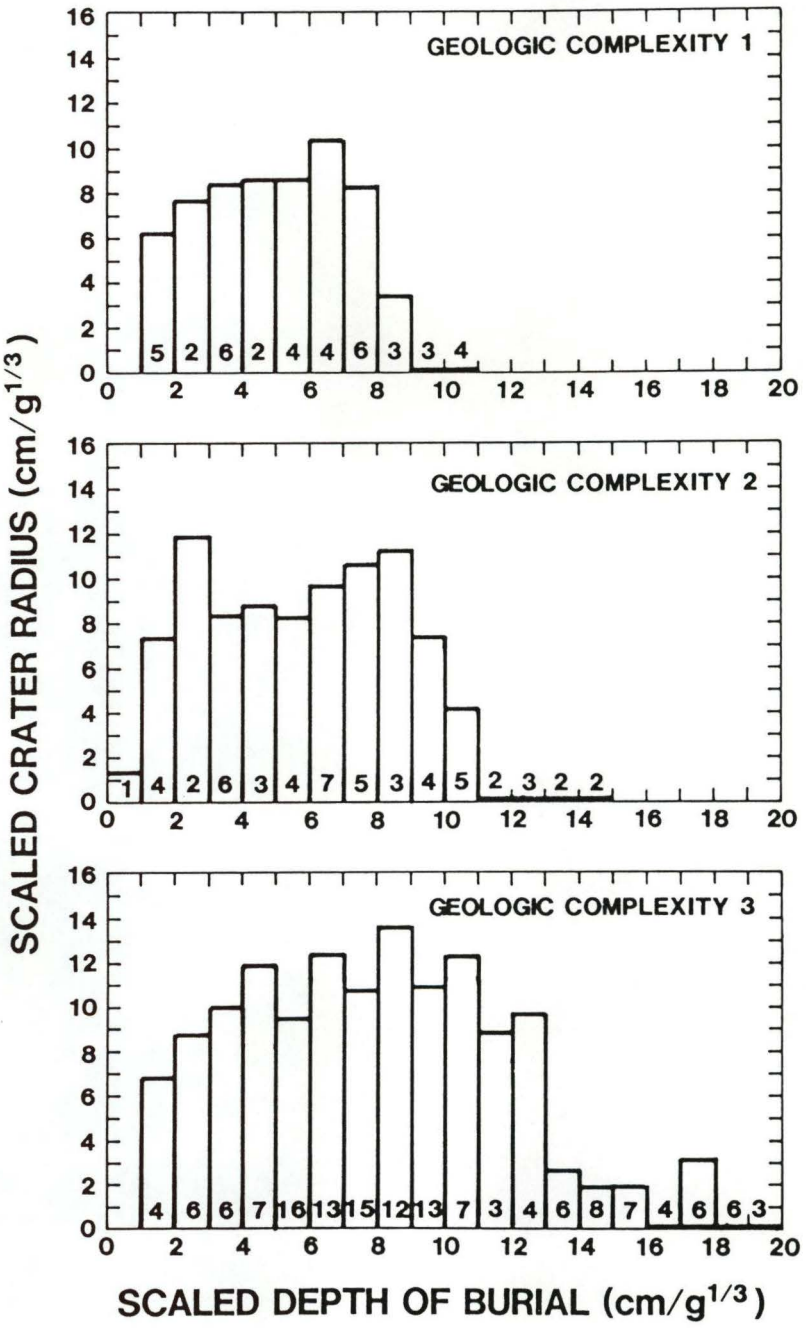
GEOLOGIC COMPLEXITY 1
5 2 6 2 4 4 6 3 3 4
GEOLOGIC COMPLEXITY 2
1 4 2 6 3 4 7 5 3 4 5 2 3 2 2
GEOLOGIC COMPLEXITY 3
4 6 6 7 16 13 15 12 13 7 3 4 6 8 7 4 6 6 3
SCALED CRATER RADIUS (cm/g^1/3)
SCALED DEPTH OF BURIAL (cm/g^1/3)

Fig. 13

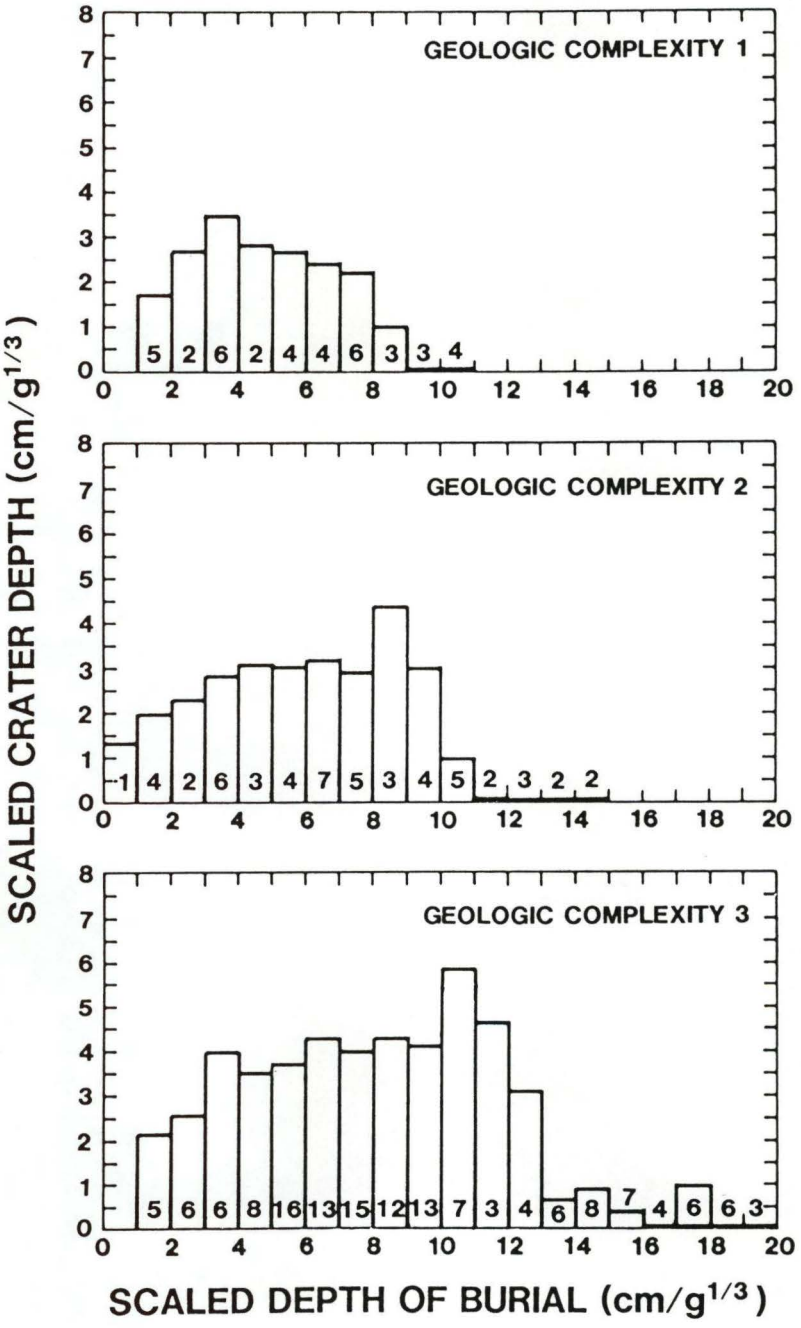
GEOLOGIC COMPLEXITY 1
5 2 6 2 4 4 6 3 3 4
GEOLOGIC COMPLEXITY 2
1 4 2 6 3 4 7 5 3 4 5 2 3 2 2
GEOLOGIC COMPLEXITY 3
5 6 6 8 16 13 15 12 13 7 3 4 6 8 7 4 6 6 3
SCALED CRATER DEPTH (cm/g^1/3)
SCALED DEPTH OF BURIAL (cm/g^1/3)

Fig. 14

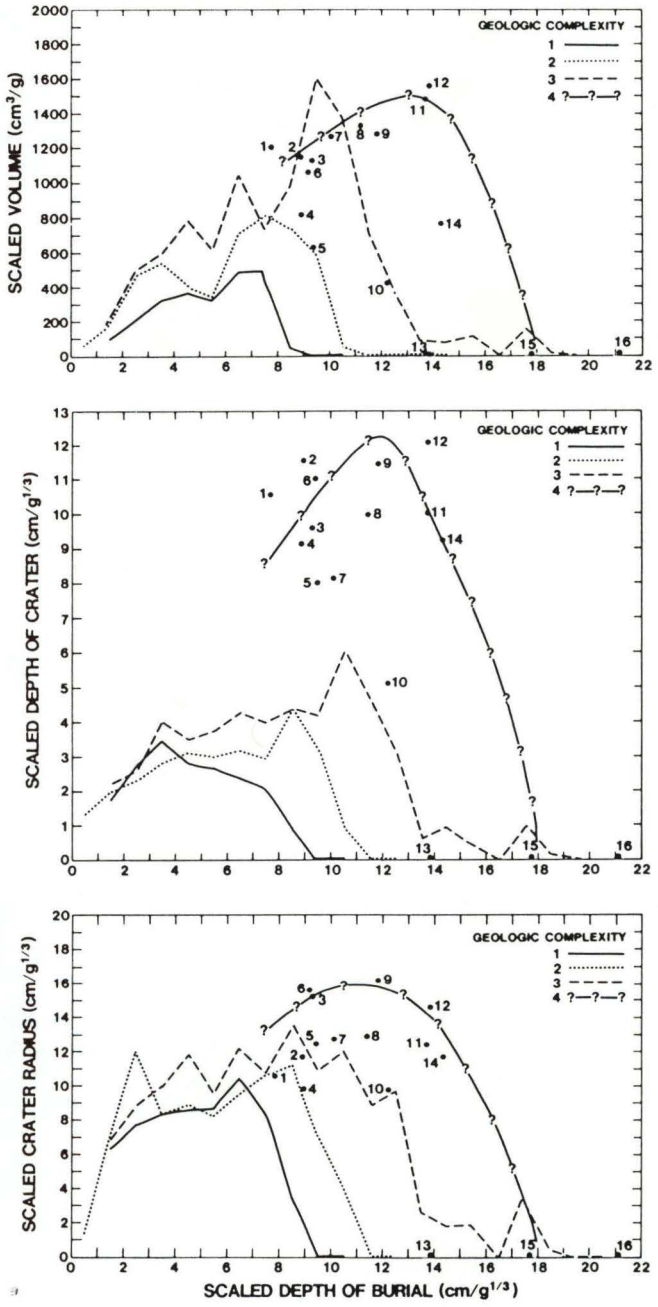
GEOLOGIC COMPLEXITY
1
2
3
4 ?—?—?
SCALED VOLUME (cm³/g)
SCALED DEPTH OF CRATER (cm/g^1/3)
SCALED CRATER RADIUS (cm/g^1/3)
SCALED DEPTH OF BURIAL (cm/g^1/3)

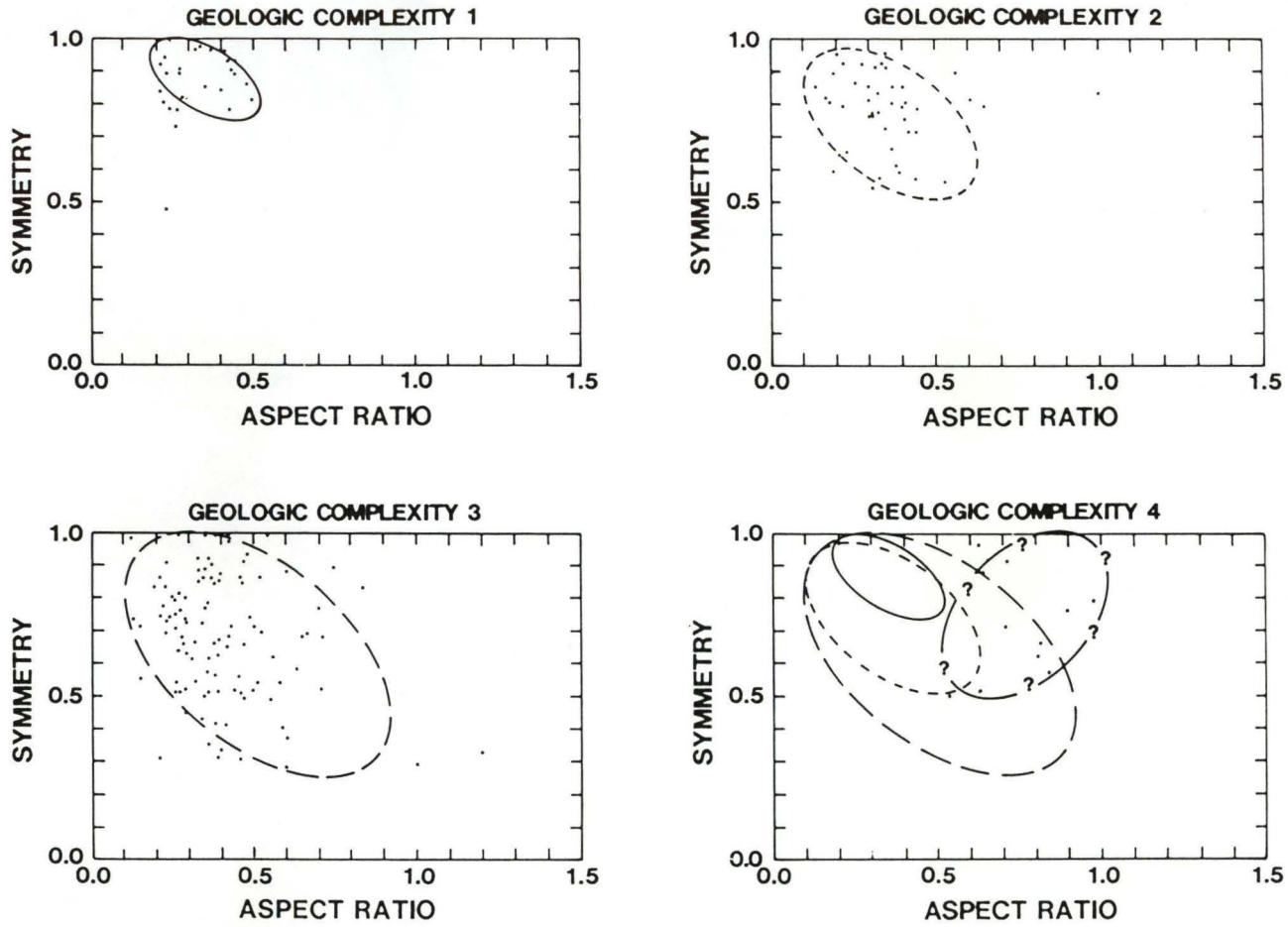
GEOLOGIC COMPLEXITY 1
GEOLOGIC COMPLEXITY 2
GEOLOGIC COMPLEXITY 3
GEOLOGIC COMPLEXITY 4
SYMMETRY
ASPECT RATIO
1.0
0.5
0.0
0.0
0.5
1.0
1.5
?

Fig. 15